GEOPHYSICS, VOL. 90, NO. 2 (MARCH-APRIL 2025); P. 1–11, 17 FIGS.
10.1190/GEO2024-0148.1

Unsupervised ground-roll attenuation via implicit neural representations

Ji Li[1], Dawei Liu[2], and Mauricio D. Sacchi[2]

ABSTRACT

Coherent noise attenuation in land seismic data is particularly challenging, especially when dealing with ground roll. Unlike incoherent noise, ground roll overlaps with reflections in time-space and frequency-wavenumber domains, making it difficult to separate them without distorting the signal. Traditional attenuation methods often struggle with this overlap, leading to a trade-off between preserving the reflections and effectively reducing noise. Recent advances in deep learning offer promising alternatives, but many rely on supervised learning, which requires a substantial amount of paired training data, which is often unavailable in real-world scenarios. Unsupervised approaches, although avoiding the need for labeled data, frequently face issues such as convergence instability and extensive parameter tuning. We develop an unsupervised deep-learning framework for separating reflections from ground roll to address these challenges. Our method leverages the inherent low-frequency bias of implicit neural representations, which emphasizes self-similarity features during training. The network initially learns to represent smoother, flattened events in seismic data before focusing on features with deeper dips and incoherent noise. To enhance the network's ability to capture the self-similarity of reflections, we apply a normal moveout (NMO) correction to flatten the reflections before using the network to extract these features from the NMO-corrected data. We further incorporate a horizontal derivative regularization term into the loss function. This term penalizes horizontal variations, ensuring a more stable convergence and reducing the burden of parameter tuning, thereby eliminating the need for early stopping. Our approach is validated with synthetic and real land data examples and compared against traditional *f-k* filtering methods. The results demonstrate its power in effectively attenuating noise while preserving the integrity of seismic reflections.

INTRODUCTION

Ground-roll attenuation remains a significant challenge in land seismic data processing. Ground roll is characterized by its dispersive nature (Al-Husseini et al., 1981) and exhibits low frequency, low velocity, and high amplitude, which makes it a form of coherent noise that can overwhelm seismic records (Saatcilar and Canitez, 1988; Beresford-Smith and Rango, 1989; Linville and Meek, 1995). This noise often dominates near-source traces, masking the weaker reflections critical for accurate subsurface imaging. Although acquisition techniques like the stackarray can partially reduce ground roll (Morse and Hildebrandt, 1989), a considerable amount typically remains on seismic records, requiring advanced signal-processing methods for further attenuation to achieve the precise imaging of subsurface structures.

Several techniques have been developed over time to mitigate ground roll noise effectively. Among these, band-pass filtering is a straightforward method, effectively separating ground roll and primary reflections based on their frequency characteristics. For instance, Saatcilar and Canitez (1988) propose distinguishing ground roll from reflections using 1D linear frequency-modulated match filters. Another viable approach is the implementation of an *f-k* filter, as demonstrated by Treitel et al. (1967) and Beresford-Smith and Rango (1989). Alternative strategies for ground-roll attenuation involve using different transforms, such as the S-transform (Askari and Siahkoohi, 2008), wavelet transform (Deighan and Watts, 1997; Wang et al., 2012; Chen et al., 2017), curvelet transform (Yarham et al., 2006; Naghizadeh and Sacchi, 2018), and radial trace transform (Henley, 2003). In addition, methods such as singular value decomposition (SVD) filtering (Porsani et al., 2010) and matching filtering (Jiao et al., 2015) have effectively eliminated ground roll. However, in real data scenarios, the efficacy of transform-based methods is often limited by the overlap between the reflections

Manuscript received by the Editor 1 March 2024; revised manuscript received 22 October 2024; published ahead of production 25 November 2024.
[1]University of Calgary, Department of Earth, Energy and Environment, Calgary, Alberta, Canada. E-mail: li.ji1@ucalgary.ca.
[2]University of Alberta, Department of Physics, Edmonton, Alberta, Canada. E-mail: 409791715@qq.com (corresponding author); msacchi@ualberta.ca.

and ground roll within the transform domains. Furthermore, spatial aliasing poses a significant challenge for frequency domain techniques, requiring methods that tolerate aliasing.

In recent years, the application of deep learning in seismic data processing has received substantial attention. Many applications of deep learning to seismic data processing have been proposed, such as the attenuation of random noise (Liu et al., 2018, 2020; Sun et al., 2022a), simultaneous source processing (Sun et al., 2022b; Wang et al., 2022b, 2023), and seismic interpolation (Oliveira et al., 2018; Wang et al., 2019; Kaur et al., 2021). Deep learning methods have also been proposed to tackle coherent noise attenuation, such as ground roll (Li et al., 2018; Kaur et al., 2020; Liu et al., 2022, 2023a), strong background noise interferences (Liu et al., 2023b), and multiples (Wang et al., 2022a). These methodologies generally fall into two categories: supervised and unsupervised. Supervised learning typically necessitates a substantial amount of clean-noisy data pairs for effective training, a challenging requirement to fulfill when processing field seismic data. In general, the network performance is constrained by its labels, rarely surpassing them significantly. However, unsupervised learning methods have the advantage of extracting the features directly from the noisy data. Nevertheless, most unsupervised methods are tailored for handling incoherent noise (Zhang et al., 2019; Li et al., 2024). Addressing coherent noise through unsupervised methods poses challenges, particularly in guaranteeing convergence (Liu et al., 2023a) and proper parameter selection (Guo et al., 2020; Pham and Li, 2022).

The implicit neural representation (INR) method (Sitzmann et al., 2020) has recently gained attention as a powerful signal processing approach. It uses a multilayer perceptron (MLP) (Almeida, 2020) architecture composed of linear layers and element-wise nonlinear activation functions. Unlike convolutional neural networks (CNNs), INRs are free from locality biases (Sitzmann et al., 2020), allowing them to capture global structures in the data more effectively. This attribute has contributed to the success of INRs across various applications, such as surface representation (Sitzmann et al., 2020), volume rendering (Martin-Brualla et al., 2021; Mildenhall et al., 2021), and generative modeling (Chan et al., 2021). Similar to other deep-learning models, INRs tend to learn low-frequency features first, a property known as the spectral bias (Rahaman et al., 2019; Xu et al., 2019; Yüce et al., 2022). This bias means the network tends to capture self-similar, smoother patterns in the data before focusing on more complex or high-frequency details (Ulyanov et al., 2018; Zhang et al., 2021). In seismic data analysis, this results in the network learning to represent flattened events, such as reflections, before addressing features with steeper dips. Incoherent noise, being more complex, is typically learned at subsequent stages of training. The effective separation of reflections and noise thus relies on selecting the appropriate point for early stopping. However, current research still needs to fully address the challenges of determining the optimal number of training iterations (Liu et al., 2023a).

This study presents a new, unsupervised deep-learning approach designed to effectively separate the reflections from the ground roll and other sources of incoherent noise in seismic data. Our method is founded upon INR using sinusoidal activation functions, strategically harnessing the inherent low-frequency bias of INR to prioritize learning self-similarity features present in the reflections over the ground roll and incoherent noise. We integrate the normal moveout (NMO) correction into our approach to flatten the reflections and enhance the separation efficacy, thereby augmenting their self-similarity. In addition, to prevent the network from inadvertently learning the ground roll during further training iterations, we introduce a quadratic regularization term based on the derivative of the extracted data along the horizontal axis into the loss function. This regularization term penalizes horizontal variations in the extracted data, preventing the network from learning unflattened events such as the ground roll. Through comprehensive evaluation using synthetic and field data examples, our proposed method successfully and effectively isolates the reflections from the ground roll and other incoherent noise sources with stable convergence, preserving the integrity of valuable reflections with minimal signal leakage.

THEORY

Implicit neural representation

INR is characterized by a pixel-wise continuous learning process and mapping input coordinates $\mathbf{c}$ to the corresponding signal values $d_{\mathbf{c}}$ through gradient descent, aiming to minimize a distortion measure such as the mean-squared error. This continuous parameterization characteristic of INRs enables storing signals at a consistent memory cost, irrespective of spatial resolution. This feature distinguishes INRs from other deep-learning techniques in reconstructing high-dimensional seismic signals, such as 5D data, a task traditionally challenging for conventional CNNs due to a high computational cost.

Unlike other deep-learning networks, INRs exhibit a pronounced spectral bias toward lower frequencies, meaning the network tends to learn self-similar, low-frequency features before capturing more complex, high-frequency components. Appropriately leveraging this bias can make INRs effective for separating different signal components, mainly when focusing on smooth data structures. However, this bias toward a narrow frequency range with limited resolution can restrict the broader applicability of INRs. To address this limitation, several methods have been developed to extend the frequency range that INRs can represent while still retaining their ability to extract self-similar features. For example, Tancik et al. (2020) propose adding a Fourier mapping layer before the MLP, which helps the network learn higher-frequency components more effectively.

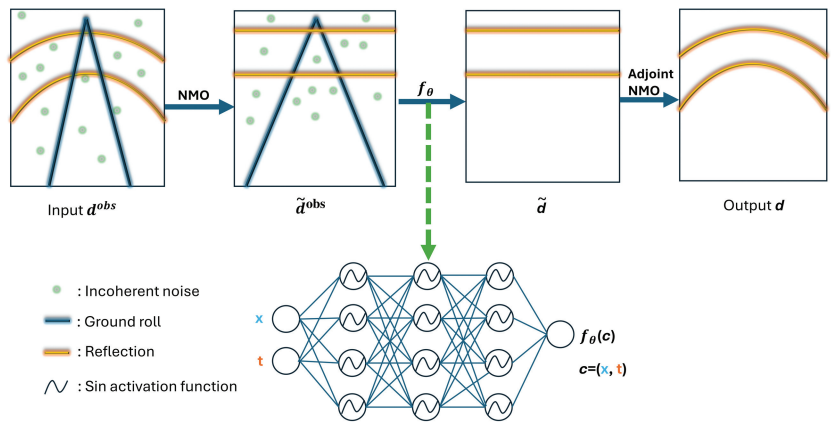

Figure 1. An illustration of the proposed ground-roll separation method framework.

Similarly, Sitzmann et al. (2020) suggest using an MLP with sinusoidal activations, which biases the network toward capturing a wider range of frequencies. Both approaches aim to enhance the ability of INRs to model complex, high-frequency variations in the data while maintaining their strengths in representing the underlying structures.

The architecture of the INR with a sinusoidal activation function can be delineated as follows:

$$f_\theta(\mathbf{c}) = \mathbf{W}^{(L)}\mathbf{z}^{(L-1)} + \mathbf{b}^{(L)}, \tag{1}$$

where

$$\begin{cases} \mathbf{z}^{(0)} = \sin(\omega_0(\mathbf{W}^{(0)}\mathbf{c} + \mathbf{b}^{(0)})) \\ \mathbf{z}^{(\ell)} = \sin(\mathbf{W}^{(\ell)}\mathbf{z}^{(\ell-1)} + \mathbf{b}^{(\ell)}), \quad \ell = 1, \ldots, L-1 \end{cases}. \tag{2}$$

Here, $\mathbf{c}$ represents the input coordinate to the first layer $\mathbf{z}^{(0)}$, which is succeeded by multiple layers of an MLP, denoted as $\mathbf{z}^{(\ell)}$. Each layer is defined by its respective weights $\mathbf{W}^{(\ell)}$ and biases $\mathbf{b}^{(\ell)}$. A sinusoidal activation function is applied element-wise at each layer $\ell = 1, \ldots, L-1$. The constant ω_0 is used for parameter rescaling at the initial stage. A larger ω_0 biases the network toward higher frequencies, effectively mitigating the low-frequency spectral bias inherent in traditional neural networks.

INR for ground-roll attenuation

As previously discussed, the low-frequency bias of INRs aids in capturing self-similarity features at early training stages, which can be leveraged to separate reflections from the ground roll. However, similar dips in the reflections and ground roll produce indistinguishable features, thus complicating separation efforts based on self-similarities. One approach is to use an NMO correction on the common-midpoint gather, which effectively flattens the reflections and enhances their self-similarity. Similar techniques have been used in traditional methods. For example, Porsani et al. (2010) demonstrate that applying the SVD method to the flattened reflections post-NMO correction yielded better results than the conventional *f-k* filter. In addition, Chiu (2013) proposes a technique to improve ground-roll attenuation by incorporating NMO into multichannel singular spectrum analysis.

The final framework of our proposed method is shown in Figure 1. We first apply the NMO correction to the observed data $\mathbf{d}^{\text{obs}}$ to flatten the reflections. Subsequently, the NMO-corrected data $\tilde{\mathbf{d}}^{\text{obs}}$ are trained by the network f_θ to separate the flattened reflections from the ground roll and all other incoherent noise. The network f_θ adopts an INR architecture based on MLP with a sinusoidal activation function, aiming to minimize a suitable loss function, which will be elaborated upon subsequently. Ultimately, we apply the adjoint NMO correction to revert the reflections to their original form.

Figure 2a shows a simple 2D synthetic example featuring three reflections and a dispersive ground roll. This example, also corrupted by incoherent noise, includes random and erratic noise. The NMO corrected data are

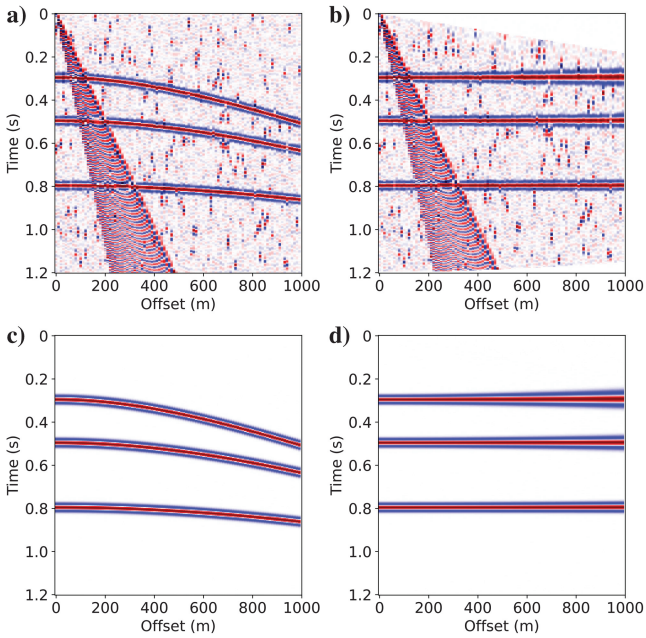

Figure 2. (a) The 2D synthetic example with three reflections and a dispersive ground roll, (b) the NMO corrected data, (c) the original reflections, and (d) the NMO corrected reflections.

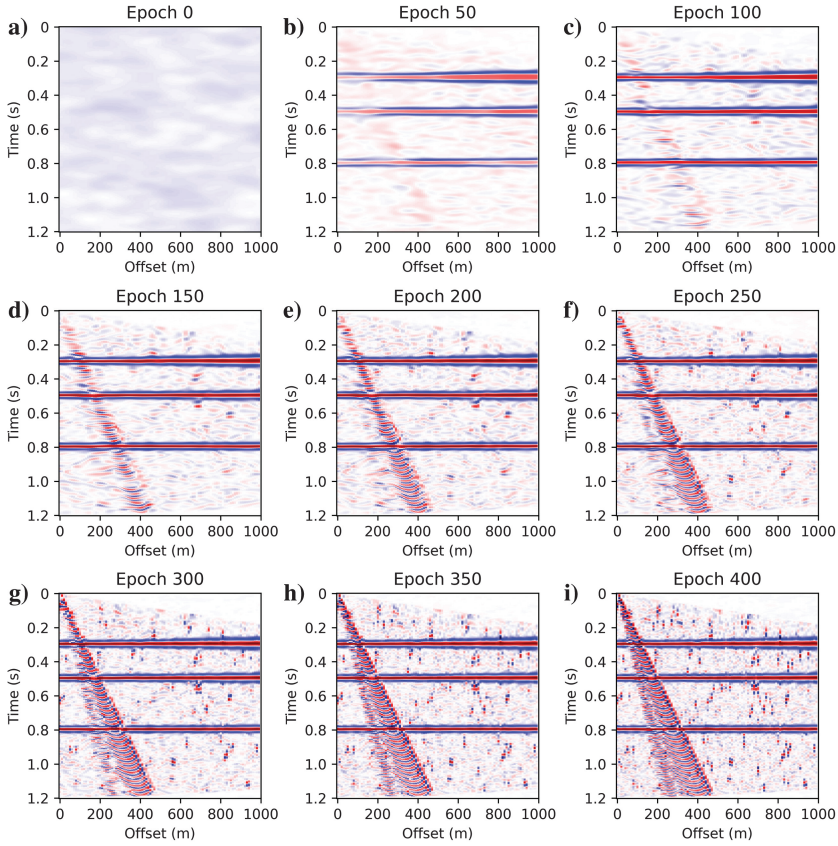

Figure 3. Reconstructed results at each stage with the ℓ_2-norm loss function.

shown in Figure 2b. We also show the original and NMO-corrected reflections in Figure 2c and 2d as references to evaluate the denoising performance of the network.

Initially, we apply the MLP network to minimize the following loss function:

$$\min_{\theta} \sum_{c \in \mathcal{C}} (f_\theta(\mathbf{c}) - \tilde{\mathbf{d}}^{\text{obs}}(\mathbf{c}))^2, \tag{3}$$

where f_θ represents the INR network parameterized by a set of weights θ. The vector $\mathbf{c}$ denotes a coordinate sample of the observed data points from the coordinate set $\mathcal{C}$, and $\tilde{\mathbf{d}}^{\text{obs}}(\mathbf{c})$ represents the observed data amplitude value after the NMO correction at $\mathbf{c}$. Figure 3 shows the learning output at each stage using the ℓ_2-norm loss function with the fixed learning rate 10^{-4}. Initially, as shown in Figure 3, the network focuses on extracting the flattened event. However, with further training iterations, it progressively reconstructs the ground roll and other noise. The results reveal that the network predominantly extracts flattened events during the early stages while partially reconstructing the ground roll and incoherent noise. This observation aligns with deep image prior-based methods (Liu et al., 2023a), wherein selecting an appropriate iteration proves challenging.

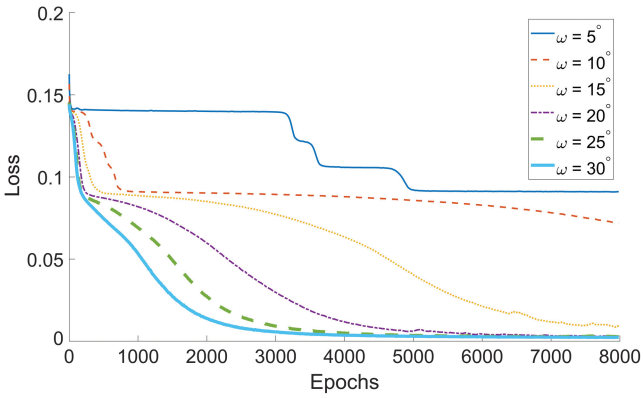

Figure 4. The loss versus the epochs for varying ω_0 values.

In contrast to the deep image prior, the parameter ω_0 in INR functions as a regulator for the initial frequency spectrum. Consequently, adjusting the ω_0 value can enhance the network's resistance against low-frequency ground-roll interference. Other high-frequency noise can be eliminated similarly by biasing it toward low-frequency features. Figure 4 shows the impact of varying ω_0 on the loss curve. In this experiment, we use a reduced learning rate of 2×10^{-5}, facilitating the slower learning of the ground roll and noise for enhanced observation. This is also a trick in the deep image before identifying the optimal early stopping iterations. This figure shows that reducing ω_0 results in increased resistance to the ground roll and incoherent noise. For example, setting ω_0 equal to 5 rad/s extends a stable stage during which the network refrains from extracting the ground roll. This occurs because reducing ω_0 narrows the network's output diversity, favoring the extraction of more straightforward self-similarity features. However, although tunning ω_0 helps us to extract the reflections better, it notably slows down the convergence rate. Moreover, although stable in a prolonged initial stage, extended training ultimately causes the network to reconstruct the ground roll, still necessitating the implementation of "loose" early stopping. Figure 5 shows the progression at each stage with $\omega_0 = 5$ rad/s, highlighting the network's gradual learning of the ground roll, which becomes evident after approximately 5000 epochs.

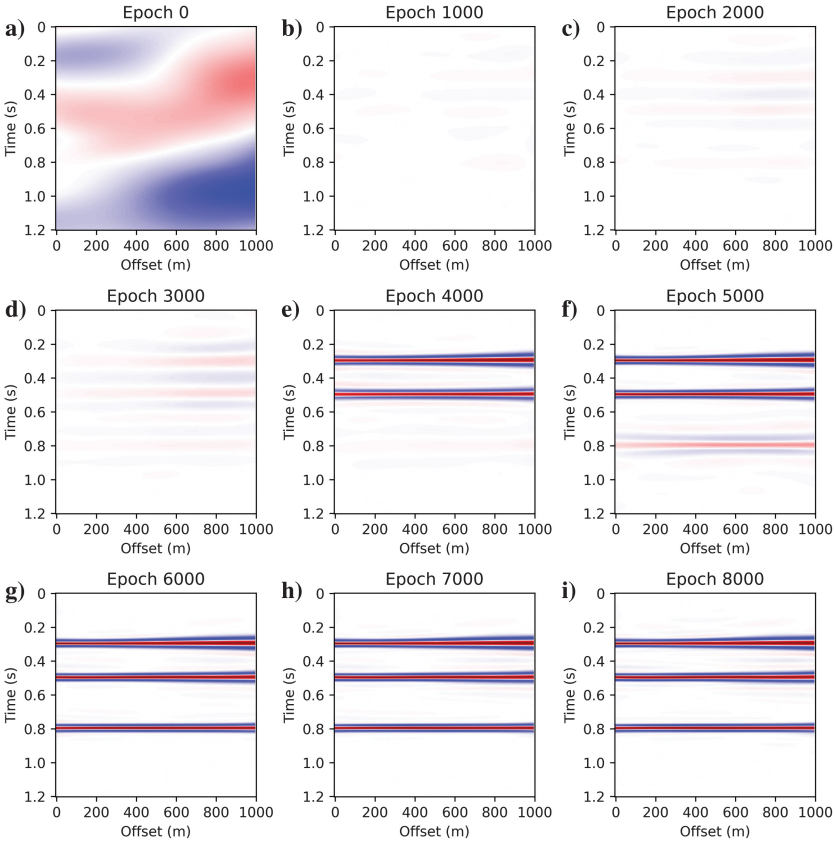

Figure 5. The reconstructed results at each stage with $\omega_0 = 5$ rad/s.

To enhance our network's robustness against the ground roll, we draw upon the traditional denoising methods and integrate the regularization techniques. Given the observed data after the NMO corrections $\tilde{\mathbf{d}}^{\text{obs}}$ and the reconstructed NMO data $\tilde{\mathbf{d}}$, we formulate the denoising problem as follows:

$$\min \|\tilde{\mathbf{d}}^{\text{obs}} - \tilde{\mathbf{d}}\|_2^2 + \mu R(\tilde{\mathbf{d}}), \tag{4}$$

where $R(\tilde{\mathbf{d}})$ represents the regularization term and μ is the trade-off parameter controlling its influence. In our context, we aim to isolate horizontal reflections in the reconstructed data $\tilde{\mathbf{d}}$. Accordingly, we introduce a regularization term penalizing horizontal variations. One straightforward approach is to use a derivative operator D_x along the horizontal offset axis x. There are two classical methods to incorporate this operator: using either $\|D_x\mathbf{d}\|_2^2$ or $\|D_x\mathbf{d}\|_1$. The ℓ_2-norm transforms the problem into a typical quadratically regularized denoising problem, whereas the ℓ_1-norm leads to the total variation solution

(Rudin et al., 1992). In our scenario, to maintain a smooth amplitude-variation-with-offset response without introducing sparsity in the solution along the offset direction, we opt for $\|D_x\mathbf{d}\|_2^2$. Consequently, the optimization function becomes

$$\min \|\tilde{\mathbf{d}}^{\text{obs}} - \tilde{\mathbf{d}}\|_2^2 + \mu\|D_x\tilde{\mathbf{d}}\|_2^2. \quad (5)$$

Considering $\tilde{\mathbf{d}}$ as the reconstructed data equal to $f_\theta(\mathbf{c})$, the final loss function for the network is given by

$$\min_\theta \sum_{c\in\mathcal{C}} \{(f_\theta(\mathbf{c}) - \tilde{d}^{\text{obs}}(\mathbf{c}))^2 + \mu(D_x f_\theta(\mathbf{c}))^2\}. \quad (6)$$

Figure 6 shows the loss curve for the network with and without the regularization term, whereas Figure 7 shows the reconstructed results at different stages. Compared with Figure 5, we observe that incorporating regularization enables a stable extraction of horizontal reflections in much fewer iterations. Furthermore, the results are derived using the default value of $\omega_0 = 30$ rad/s from the original SIREN network (INR with the sinusoidal activation function) (Sitzmann et al., 2020). This underscores how regularization eases parameter tuning and frees us from relying on specific values for ω_0. They emphasize the need to incorporate the derivative regularization term into the network to extract flattened reflections exclusively.

EXAMPLES

In this section, we conduct various tests using synthetic and real land seismic data to demonstrate the effectiveness of the proposed method. Throughout the training, we use a fixed learning rate of 10^{-4} for synthetic and real data examples. Given that we are dealing with 2D data gathers, which are relatively small in size, we apply the gradient descent directly to the entire data set instead of dividing it into smaller patches with a mini-batch gradient descent. Posttraining, we use the adjoint NMO correction to revert the reflections to their original form and compare them with the original data to showcase the performance in attenuating the ground roll and minimizing signal leakage. For the 2D real data examples, we compare the proposed method with the traditional *f-k* filter, a frequently used method in the industry for ground-roll attenuation due to its effectiveness and simple implementation. In addition, we visualize the original data and the denoised results in the *f-k* domain to provide further comparisons and insights.

Synthetic example

Simple synthetic example

We initially apply the proposed method to separate the ground roll in the data set shown in Figure 2a. This data set comprises three reflections and 300 samples with a 4 ms sampling interval. In addition, it includes 100 traces with a 10 m trace interval. The ground roll, theoretically dispersive rather than linear, exhibits different phase velocities for each frequency (Le Meur et al., 2008). Consequently, in this example, we simulate the ground roll as a dispersive wave instead of linear events. The presence of erratic noise further complicates the separation task. Figure 8 shows the reconstructed reflections obtained from the NMO-corrected data in Figure 2b, along with their associated differences compared with the original reflections in Figure 2d. The proposed INR method successfully

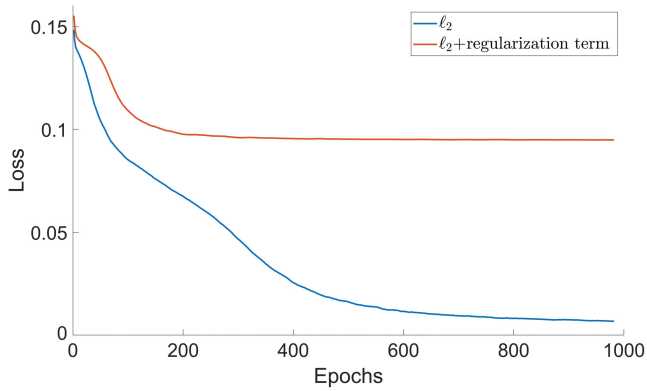

Figure 6. The comparison of the loss curves with and without the regularization term $\|D_x\tilde{\mathbf{d}}\|_2^2$.

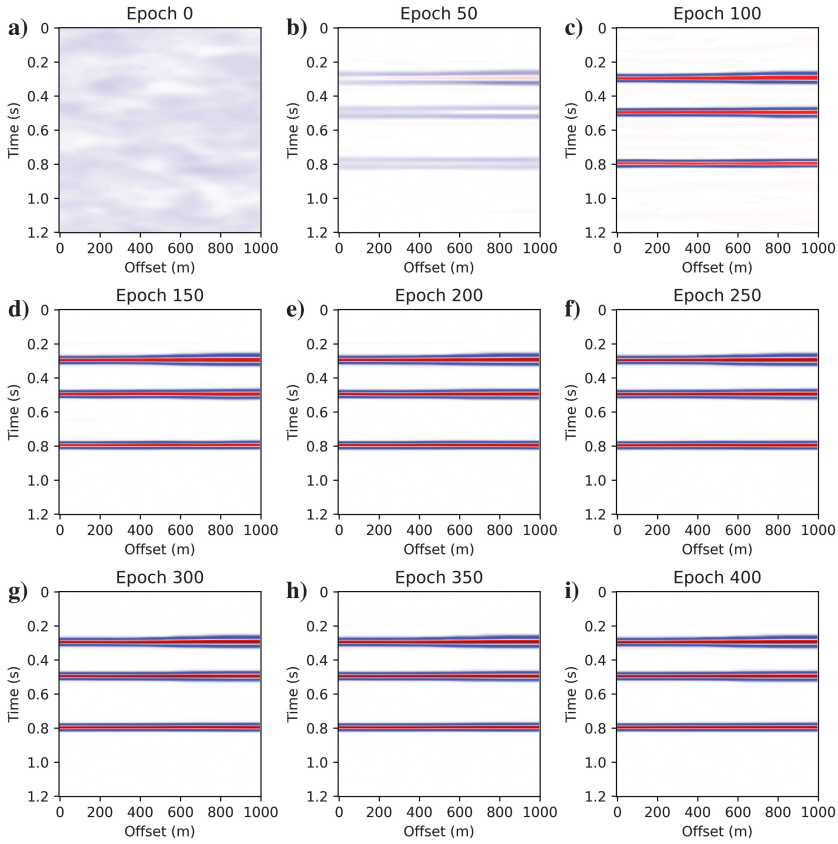

Figure 7. Reconstructed results at each stage with the ℓ_2-norm and regularization term.

separates the reflections from the heavily noisy data. The absence of visible residual reflections in the difference panel underscores the high fidelity of our method. Subsequently, we reverse the NMO to return the reconstructed reflections to their original domain. The resulting output is shown in Figure 9, along with a comparison of the errors with Figure 2c. The signal-to-noise ratio (S/N) between the reconstructed and the original reflections is 23.2 dB. Figure 9 also shows the reconstructed reflections obtained by the *f-k* filter, with the S/N equal to 6.3 dB.

We have additionally depicted the result in the *f-k* domain, as shown in Figure 10. Traditional *f-k* filters struggle to eliminate some of these coefficients due to the overlapping nature of the ground roll and reflections. The aliasing ground roll also challenges many conventional methods, such as Radon transforms (Turner, 1990). Figure 10b shows that the proposed method has effectively eliminated all the *f-k* coefficients of the ground roll and other incoherent noise.

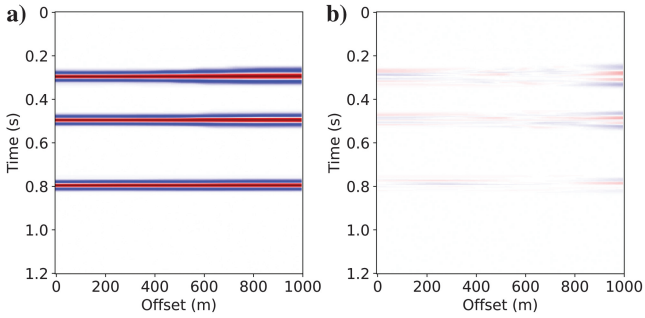

Figure 8. The reconstructed results for the NMO corrected data using the proposed INR. (a) The extracted horizontal reflections and (b) the differences relative to Figure 2d.

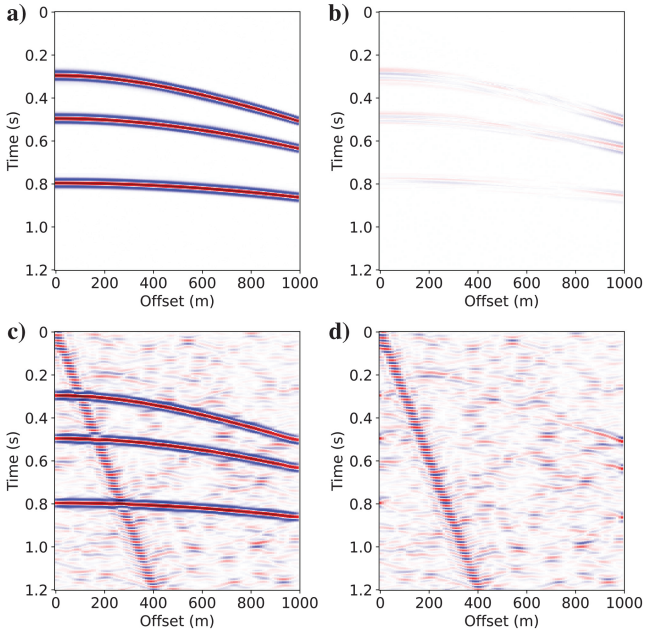

Figure 9. The final reconstructed reflections: (a) the reconstructed reflections by the proposed method, (b) the differences between (a) Figure 2c, (c) the reconstructed reflections by the *f-k* filter, and (d) the difference between (c) and Figure 2c.

The complete pattern of the ground roll in Figure 10c further evidences the successful separation achieved by our method.

Finite-difference synthetic data example

Subsequently, we evaluate the proposed method using a more complex and realistic synthetic example generated via elastic wave simulation using a finite-difference method. The velocity model incorporates intricate near-surface structures and heterogeneities. The resulting data set comprises 3801 samples with a 2 ms sampling interval. Furthermore, the data set includes 250 traces with a 32 m trace interval. The NMO-corrected shot gather is shown in Figure 11a. Figure 11b and 11c shows the separated signal and ground roll by *f-k* filter, respectively. Figure 11d and 11e shows the separated signal and ground roll by the proposed method. The corresponding *f-k* domains are shown in Figure 12. Compared with the red rectangular area signal, the proposed method successfully removes the ground roll with minimal signal leakage.

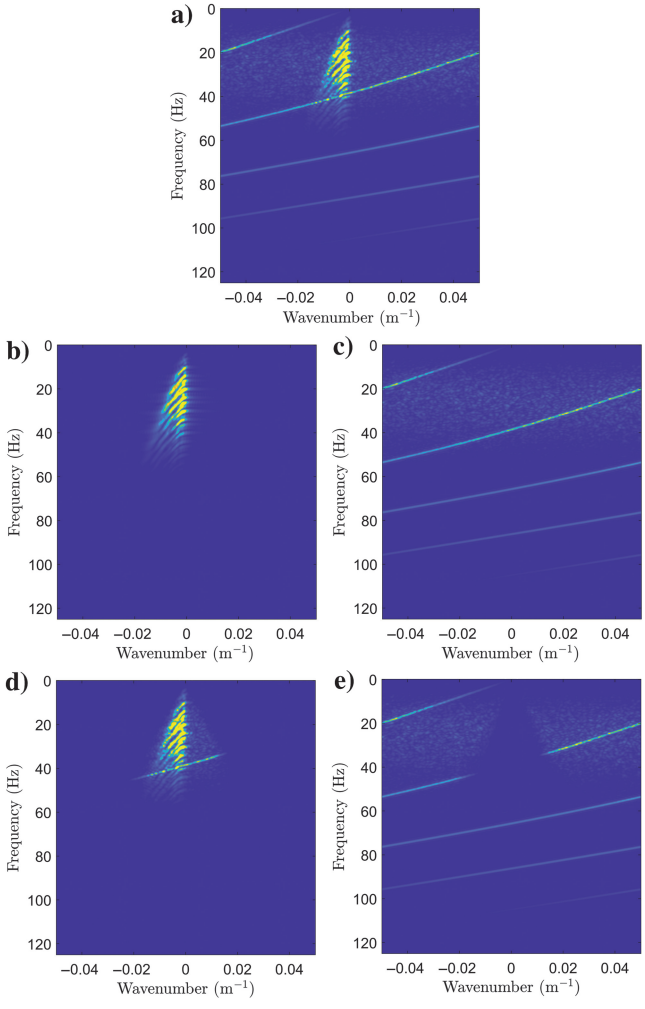

Figure 10. The *f-k* panels: (a) the original data, (b) the reconstructed reflections by the proposed method, (c) the separated noise by the proposed method, (d) the reconstructed reflections by the *f-k* filter, and (e) the separated noise by the *f-k* filter.

Real data example

In this section, we use the proposed method to eliminate the ground roll in the real data examples, consisting of two 2D examples and one 3D example. The two 2D data sets are from the open data from Oz Yilmaz. Before commencing network training, the following preprocessing is performed. First, we clip the data to reveal deep, weak events better. Next, we mute the surface refractions to reduce interference. Finally, we apply NMO to flatten the reflections. Then, we use our method to denoise the preprocessed data. Notably, using NMO correction on common-shot gathers is appropriate primarily for geologic structures with minimal dip and is an accepted practice in the industry (Perkins and Zwaan, 2000; Le Meur et al., 2008).

The first shot gather, Record 06 from the Oz Yilmaz field data set, is selected for examination. A high-amplitude ground roll significantly contaminates the near-offset traces, obscuring the reflections, as shown in Figure 13a. Figure 13c–13f compares the denoising outcomes of the *f-k* filtering and our approach. Although *f-k* filtering is effective in areas with moderate noise, it fails to adequately address the strong noise as it blurs the near-offset reflections. In contrast, our method yields denoised results with clear, continuous reflections, as shown in Figure 13e. The difference gather in Figure 13f further confirms the high fidelity of our technique, evidenced by the absence of significant signal loss. Figure 14 shows the *f-k* panels of the preceding comparative results. Figure 14a shows that the reflections and ground roll are significantly aliased and overlapping, presenting a substantial challenge for conventional processing techniques. Comparison between Figure 14b and 14c reveals that the cutoff region of *f-k* filtering is carefully selected to reduce ringing artifacts, ensuring a fair comparison. Figure 14d and 14e demonstrates that our proposed method effectively isolates the reflections from the ground roll and other land noise, even in spatial aliasing and the overlapping *f-k* features.

The second example, Record 26 from the Oz Yilmaz data set, presents unique challenges. Figure 15a shows the original common-shot gathers. Despite clipping the data, the reflections remain exceptionally weak, complicating their extraction via our

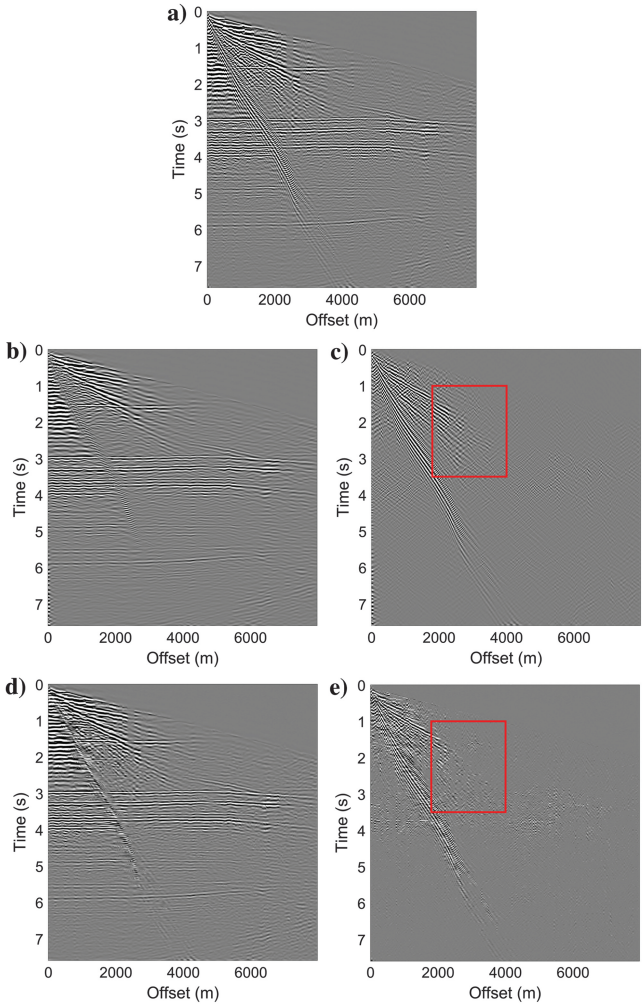

Figure 11. The NMO corrected synthetic example generated by the finite-difference method; the red boxes show that our result has less signal leakage. (a) The original data, (b) the denoised data by the *f-k* filter, (c) the separated noise by the *f-k* filter, (d) the denoised data by the proposed method, and (e) the separated noise by the proposed method.

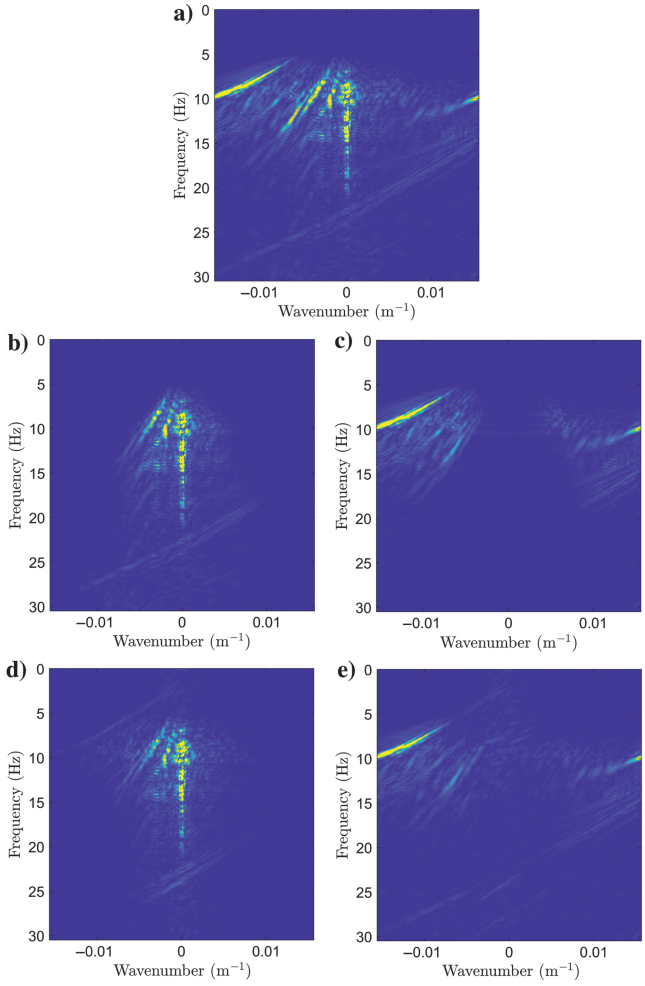

Figure 12. The corresponding *f-k* panels for the data in Figure 11.

method. Moreover, the *f-k* panel shown in Figure 16a does not clearly differentiate between the reflections and the noise, complicating the determination of the appropriate filtering boundaries. Figure 15 shows the denoised result comparison, confirming the previous conclusion that our method surpasses *f-k* filtering in preserving the reflection wavefield features. This substantial enhancement in the S/N is further evidenced in the *f-k* panels from Figure 16, wherein our method effectively extracts the reflections from the heavily noisy data. The signal in the red rectangular area demonstrates that our method better preserves the continuity of the waveforms.

The final example is a 3D field data set comprising 11 shot gathers. As shown in Figure 17, each shot gather consists of 2000 samples with a sampling interval of 2 ms. The ground roll and near-surface scattering energy dominate seismic recordings, obscuring useful signals significantly. First, we use a semblance map to estimate the reflection velocities and apply an NMO correction. We implement a loose band-pass filter for this complex data set to attenuate a portion of the ground roll while preserving the useful signal. Then, we apply the proposed method to eliminate the remaining ground roll. This is consistent with the industrial processing of complex data, which involves cascading several filters to eliminate specific noise gradually. In Figure 17b, we can observe an improvement in the S/N. Many reflections previously obscured by noise have become visible with satisfactory continuity. Further examination of the noise section in Figure 17c reveals that the ground roll and scattering have been effectively separated from the original data. Moreover, there is no evident signal leakage, demonstrating high-fidelity noise removal. This result verifies that our method is applicable for effectively distinguishing the proper signals from the ground roll in complex acquisition conditions, making it a potentially robust solution for processing large-scale prestack data with high accuracy and reliability.

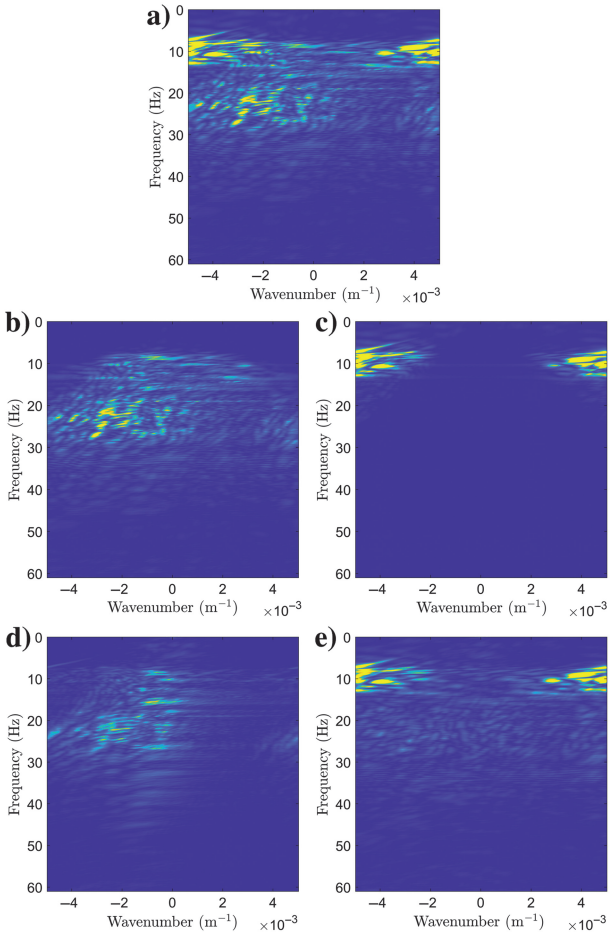

Figure 14. The corresponding *f-k* panels for the gathers presented in Figure 13. (a) The original data (muted data), (b and c) the denoised results and the separated ground roll by *f-k* filtering, and (d) and (e) the denoised results and the separated ground roll by the proposed method.

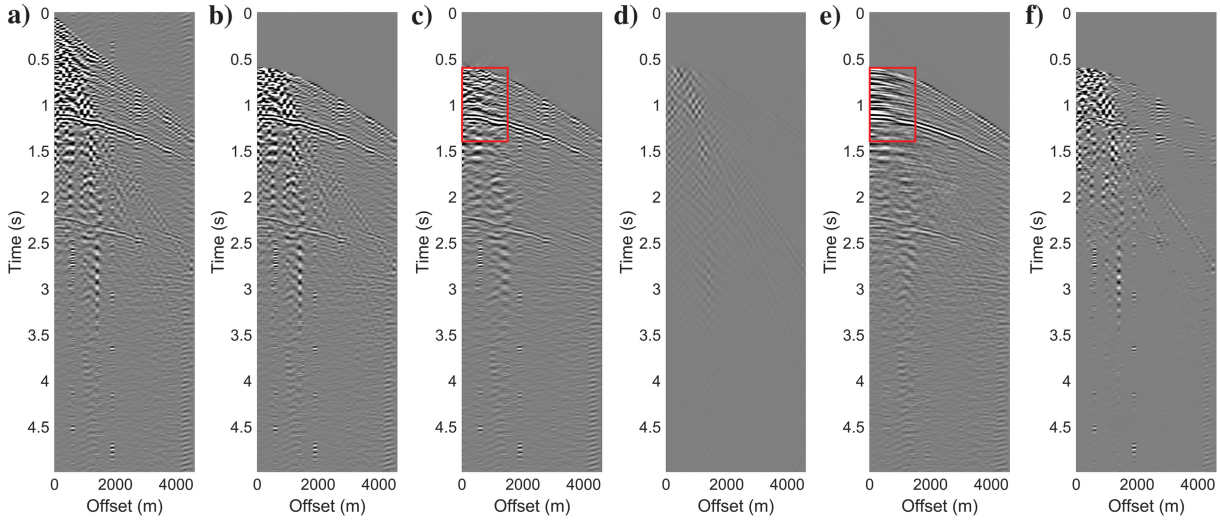

Figure 13. Record 06 from the Oz Yilmaz field data set, the red boxes show that our results produce more continuous reflections. (a) The original data, (b) the muted data, (c) the denoised results by *f-k* filtering, (d) the differences between (b and c), (e) the denoised results by the proposed method, and (f) the differences between (b and e).

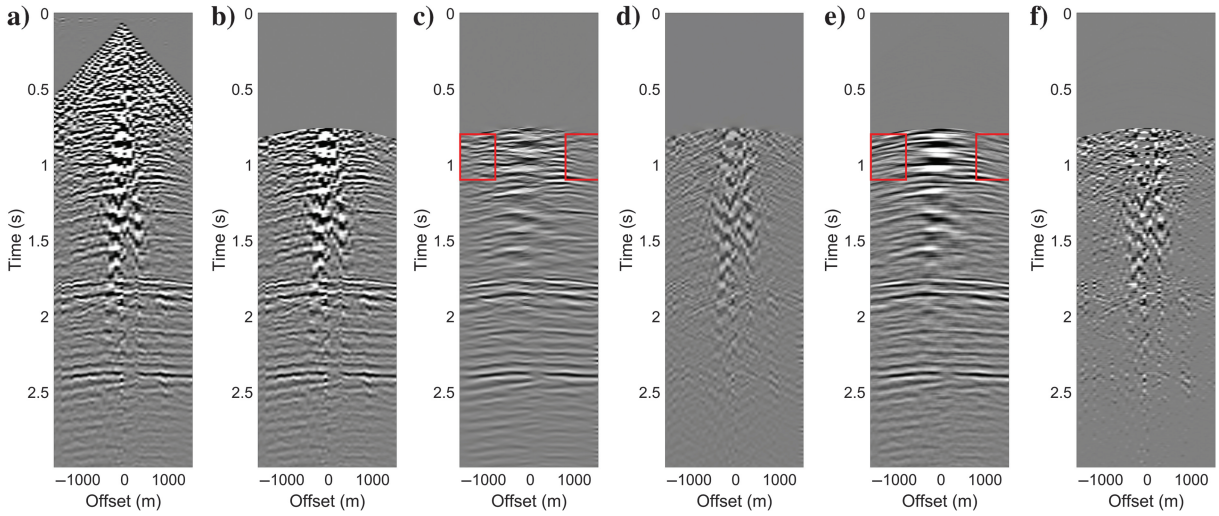

Figure 15. Record 26 from the Oz Yilmaz field data set, the red boxes show that our results produce more continuous reflections. (a) The original data, (b) the muted data, (c) the denoised results by *f-k* filtering, (d) the differences between (b and c), (e) the denoised results by the proposed method, and (f) the differences between (b and e).

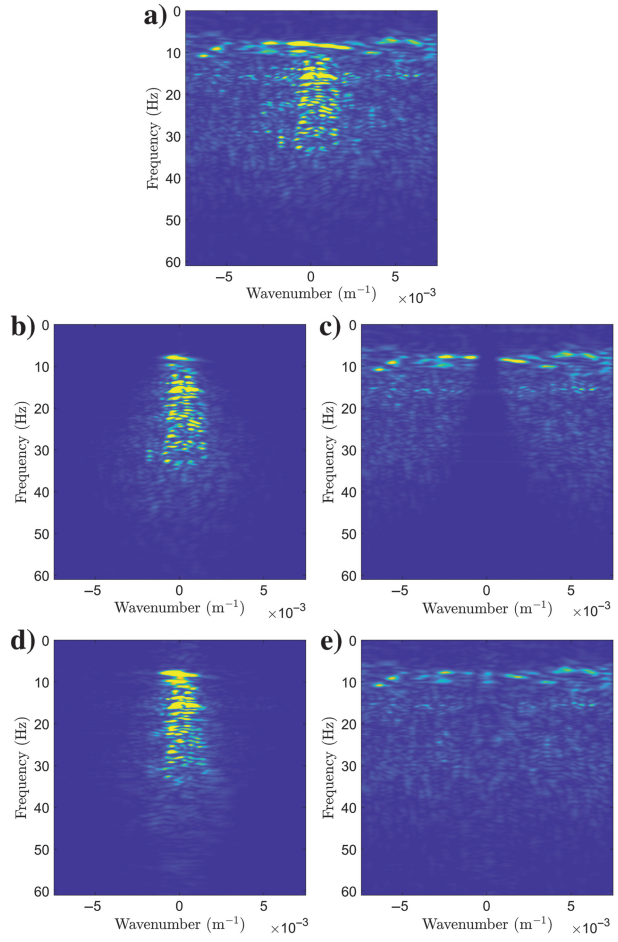

Figure 16. The corresponding *f-k* panels for the gathers presented in Figure 15. (a) The original data (muted data), (b and c) the denoised results and the separated ground roll by *f-k* filtering, and (d and e) the denoised results and the separated ground roll by the proposed method.

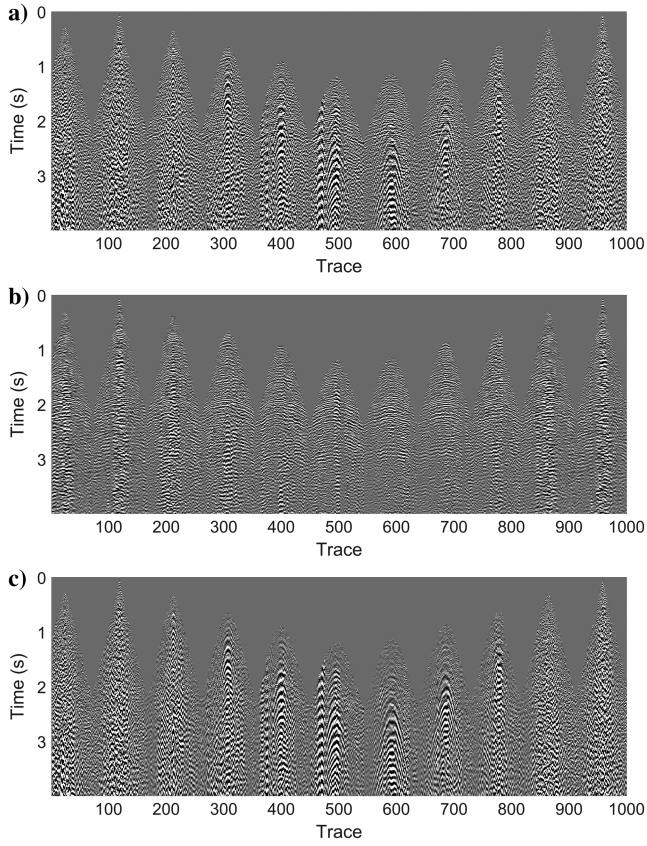

Figure 17. The 3D example: (a) the muted 3D real shot gather, (b) reconstructed reflections, and (c) separated noise (the ground roll and the scattering noise).

CONCLUSION

We present an unsupervised deep-learning approach to separate the reflections from the ground roll and the other incoherent noise.

Our method capitalizes on the inherent low-frequency bias of INRs, which can effectively extract reflections with self-similar features. To enhance the self-similarity within the reflections, we apply NMO corrections to flatten them. In addition, a regularization term is introduced, involving the derivative of the extracted data along the horizontal axis, ensuring robustness against unflattened events and guaranteeing convergence. Synthetic and real data sets are used to demonstrate the effectiveness and robustness of our proposed method. Our method performs better than traditional approaches like *f-k* filtering, particularly when reflections are aliased or weak. In this challenging context, it successfully separates the reflections from the ground roll while minimizing signal leakage. Future research efforts will address the challenges posed by the high-amplitude scattering noise associated with the ground roll around zero offsets.

ACKNOWLEDGMENTS

This work was funded by the CREWES industrial sponsors and the Natural Science and Engineering Research Council of Canada (NSERC) through grant CRDPJ 543578-19. The contribution of the second author was supported by the industrial sponsors of the Signal Analysis and Imaging Group (SAIG) consortium at the University of Alberta.

DATA AND MATERIALS AVAILABILITY

Data associated with this research are available and can be accessed via the following URL: https://seismicrocks.com/oz40.html.

REFERENCES

Al-Husseini, M. I., J. B. Glover, and B. J. Barley, 1981, Dispersion patterns of the ground roll in eastern Saudi Arabia: Geophysics, **46**, 121–137, doi: 10.1190/1.1441183.

Almeida, L. B., 2020, Multilayer perceptrons, *in* P. Samui, S. S. Roy, and V. E. Balas, eds., Handbook of neural computation: CRC Press, C1-2.

Askari, R., and H. R. Siahkoohi, 2008, Ground roll attenuation using the S and x-f-k transforms: Geophysical Prospecting, **56**, 105–114, doi: 10.1111/j.1365-2478.2007.00659.x.

Beresford-Smith, G., and R. Rango, 1989, Suppression of ground roll by windowing in two domains: First Break, **7**, 55–63, doi: 10.3997/1365-2397.1989004.

Chan, E. R., M. Monteiro, P. Kellnhofer, J. Wu, and G. Wetzstein, 2021, pi-GAN: Periodic implicit generative adversarial networks for 3D-aware image synthesis: Proceedings of the IEEE/CVF Conference on Computer Vision and Pattern Recognition, 5799–5809.

Chen, X., W. Chen, X. Wang, and W. Wang, 2017, Sparsity-optimized separation of body waves and ground-roll by constructing dictionaries using tunable Q-factor wavelet transforms with different Q-factors: Geophysical Journal International, **211**, 621–636, doi: 10.1093/gji/ggx332.

Chiu, S. K., 2013, Coherent and random noise attenuation via multichannel singular spectrum analysis in the randomized domain: Geophysical Prospecting, **61**, 1–9, doi: 10.1111/j.1365-2478.2012.01090.x.

Deighan, A. J., and D. R. Watts, 1997, Ground-roll suppression using the wavelet transform: Geophysics, **62**, 1896–1903, doi: 10.1190/1.1444290.

Guo, R., H. Maniar, H. Di, N. Moldoveanu, A. Abubakar, and M. Li, 2020, Ground roll attenuation with an unsupervised deep learning approach: 90th Annual International Meeting, SEG, Expanded Abstracts, 3164–3168, doi: 10.1190/segam2020-3425792.1.

Henley, D. C., 2003, Coherent noise attenuation in the radial trace domain: Geophysics, **68**, 1408–1416, doi: 10.1190/1.1598134.

Jiao, S., Y. Chen, M. Bai, W. Yang, E. Wang, and S. Gan, 2015, Ground roll attenuation using non-stationary matching filtering: Journal of Geophysics and Engineering, **12**, 922–933, doi: 10.1088/1742-2132/12/6/922.

Kaur, H., S. Fomel, and N. Pham, 2020, Seismic ground-roll noise attenuation using deep learning: Geophysical Prospecting, **68**, 2064–2077, doi: 10.1111/1365-2478.12985.

Kaur, H., N. Pham, and S. Fomel, 2021, Seismic data interpolation using deep learning with generative adversarial networks: Geophysical Prospecting, **69**, 307–326, doi: 10.1111/1365-2478.13055.

Le Meur, D., N. Benjamin, R. Cole, and M. Al Harthy, 2008, Adaptive groundroll filtering: 70th Annual International Conference and Exhibition, EAGE, Extended Abstracts, cp-40, doi: 10.3997/2214-4609.20147745.

Li, H., W. Yang, and X. Yong, 2018, Deep learning for ground-roll noise attenuation: 88th Annual International Meeting, SEG, Expanded Abstracts, 1981–1985, doi: 10.1190/segam2018-2981295.1.

Li, J., D. Trad, and D. Liu, 2024, Robust seismic data denoising via self-supervised deep learning: Geophysics, **89**, no. 5, V437–V451, doi: 10.1190/geo2023-0762.1.

Linville, A. F., and R. A. Meek, 1995, A procedure for optimally removing localized coherent noise: Geophysics, **60**, 191–203, doi: 10.1190/1.1443746.

Liu, D., Z. Deng, C. Wang, X. Wang, and W. Chen, 2020, An unsupervised deep learning method for denoising prestack random noise: IEEE Geoscience and Remote Sensing Letters, **19**, 1–5, doi: 10.1109/LGRS.2020.3019400.

Liu, D., M. D. Sacchi, X. Wang, and W. Chen, 2023a, Unsupervised deep learning for ground roll and scattered noise attenuation: IEEE Transactions on Geoscience and Remote Sensing, **61**, 5920613, doi: 10.1109/TGRS.2023.3325324.

Liu, D., W. Wang, W. Chen, X. Wang, Y. Zhou, and Z. Shi, 2018, Random noise suppression in seismic data: What can deep learning do?: 88th Annual International Meeting, SEG, Expanded Abstracts, 2016–2020, doi: 10.1190/segam2018-2998114.1

Liu, D., W. Wang, X. Wang, Z. Shi, M. D. Sacchi, and W. Chen, 2023b, Improving sparse representation with deep learning: A workflow for separating strong background interference: Geophysics, **88**, no. 1, WA253–WA266, doi: 10.1190/geo2022-0179.1.

Liu, D., X. Wang, X. Yang, H. Mao, M. D. Sacchi, and W. Chen, 2022, Accelerating seismic scattered noise attenuation in offset-vector tile domain: Application of deep learning: Geophysics, **87**, no. 5, V505–V519, doi: 10.1190/geo2021-0654.1.

Martin-Brualla, R., N. Radwan, M. S. Sajjadi, J. T. Barron, A. Dosovitskiy, and D. Duckworth, 2021, Nerf in the wild: Neural radiance fields for unconstrained photo collections: Proceedings of the IEEE/CVF Conference on Computer Vision and Pattern Recognition, 7210–7219.

Mildenhall, B., P. P. Srinivasan, M. Tancik, J. T. Barron, R. Ramamoorthi, and R. Ng, 2021, Nerf: Representing scenes as neural radiance fields for view synthesis: Communications of the ACM, **65**, 99–106, doi: 10.1145/3503250.

Morse, P. F., and G. F. Hildebrandt, 1989, Ground-roll suppression by the stackarray: Geophysics, **54**, 290–301, doi: 10.1190/1.1442654.

Naghizadeh, M., and M. Sacchi, 2018, Ground-roll attenuation using curvelet downscaling: Geophysics, **83**, no. 3, V185–V195, doi: 10.1190/geo2017-0562.1.

Oliveira, D. A., R. S. Ferreira, R. Silva, and E. V. Brazil, 2018, Interpolating seismic data with conditional generative adversarial networks: IEEE Geoscience and Remote Sensing Letters, **15**, 1952–1956, doi: 10.1109/LGRS.2018.2866199.

Perkins, C., and M. Zwaan, 2000, Ground roll attenuation: 62nd Annual International Conference and Exhibition, EAGE, Extended Abstracts, cp-28, doi: 10.3997/2214-4609-pdb.28.L21.

Pham, N., and W. Li, 2022, Physics-constrained deep learning for ground roll attenuation: Geophysics, **87**, no. 1, V15–V27, doi: 10.1190/geo2020-0691.1.

Porsani, M. J., M. G. Silva, P. E. Melo, and B. Ursin, 2010, SVD filtering applied to ground-roll attenuation: Journal of Geophysics and Engineering, **7**, 284–289, doi: 10.1088/1742-2132/7/3/007.

Rahaman, N., A. Baratin, D. Arpit, F. Draxler, M. Lin, F. Hamprecht, Y. Bengio, and A. Courville, 2019, On the spectral bias of neural networks: International Conference on Machine Learning, 5301–5310.

Rudin, L. I., S. Osher, and E. Fatemi, 1992, Nonlinear total variation based noise removal algorithms: Physica D: Nonlinear Phenomena, **60**, 259–268, doi: 10.1016/0167-2789(92)90242-F.

Saatcilar, R., and N. Canitez, 1988, A method of ground-roll elimination: Geophysics, **53**, 894–902, doi: 10.1190/1.1442526.

Sitzmann, V., J. Martel, A. Bergman, D. Lindell, and G. Wetzstein, 2020, Implicit neural representations with periodic activation functions: Advances in Neural Information Processing Systems, 7462–7473.

Sun, H., F. Yang, and J. Ma, 2022a, Seismic random noise attenuation via self-supervised transfer learning: IEEE Geoscience and Remote Sensing Letters, **19**, 1–5, doi: 10.1109/LGRS.2022.3146173.

Sun, J., S. Hou, V. Vinje, G. Poole, and L.-J. Gelius, 2022b, Deep learning-based shot-domain seismic deblending: Geophysics, **87**, no. 3, V215–V226, doi: 10.1190/geo2020-0865.1.

Tancik, M., P. Srinivasan, B. Mildenhall, S. Fridovich-Keil, N. Raghavan, U. Singhal, R. Ramamoorthi, J. Barron, and R. Ng, 2020, Fourier features let networks learn high frequency functions in low dimensional domains: Advances in Neural Information Processing Systems, 7537–7547.

Treitel, S., J. L. Shanks, and C. W. Frasier, 1967, Some aspects of fan filtering: Geophysics, **32**, 789–800, doi: 10.1190/1.1439889.

Turner, G., 1990, Aliasing in the tau-p transform and the removal of spatially aliased coherent noise: Geophysics, **55**, 1496–1503, doi: 10.1190/1.1442797.

Ulyanov, D., A. Vedaldi, and V. Lempitsky, 2018, Deep image prior: Proceedings of the IEEE Conference on Computer Vision and Pattern Recognition, 9446–9454.

Wang, B., N. Zhang, W. Lu, and J. Wang, 2019, Deep-learning-based seismic data interpolation: A preliminary result: Geophysics, **84**, no. 1, V11–V20, doi: 10.1190/geo2017-0495.1.

Wang, K., T. Hu, and S. Wang, 2023, Iterative deblending using unsupervised learning with double-deep neural networks: Geophysics, **88**, no. 3, V187–V205, doi: 10.1190/geo2022-0299.1.

Wang, K., T. Hu, and B. Zhao, 2022a, An unsupervised deep neural network approach based on ensemble learning to suppress seismic surface-related multiples: IEEE Transactions on Geoscience and Remote Sensing, **60**, 1–14, doi: 10.1109/TGRS.2022.3225809.

Wang, S., W. Hu, P. Yuan, X. Wu, Q. Zhang, P. Nadukandi, G. O. Botero, and J. Chen, 2022b, A self-supervised deep learning method for seismic data deblending using a blind-trace network: IEEE Transactions on Neural Networks and Learning Systems, **34**, 3405–3414, doi: 10.1109/TNNLS.2022.3188915.

Wang, W., J. Gao, W. Chen, and J. Xu, 2012, Data adaptive ground-roll attenuation via sparsity promotion: Journal of Applied Geophysics, **83**, 19–28, doi: 10.1016/j.jappgeo.2012.04.004.

Xu, Z.-Q. J., Y. Zhang, and Y. Xiao, 2019, Training behavior of deep neural network in frequency domain: 26th International Conference on Neural Information Processing, 264–274.

Yarham, C., U. Boeniger, and F. Herrmann, 2006, Curvelet-based ground roll removal: 76th Annual International Meeting, SEG, Expanded Abstracts, 2777–2782, doi: 10.1190/1.2370101.

Yüce, G., G. Ortiz-Jiménez, B. Besbinar, and P. Frossard, 2022, A structured dictionary perspective on implicit neural representations: Proceedings of the IEEE/CVF Conference on Computer Vision and Pattern Recognition, 19228–19238.

Zhang, C., S. Bengio, M. Hardt, B. Recht, and O. Vinyals, 2021, Understanding deep learning (still) requires rethinking generalization: Communications of the ACM, **64**, 107–115, doi: 10.1145/3446776.

Zhang, M., Y. Liu, and Y. Chen, 2019, Unsupervised seismic random noise attenuation based on deep convolutional neural network: IEEE Access, **7**, 179810–179822, doi: 10.1109/ACCESS.2019.2959238.

Biographies and photographs of the authors are not available.